On: 13 November 2014, At: 02:38
Publisher: Taylor & Francis
Informa Ltd Registered in England and Wales Registered Number: 1072954 Registered office: Mortimer House, 37-41 Mortimer Street, London W1T 3JH, UK

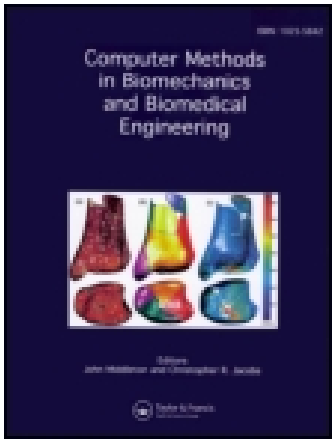

Computer Methods in Biomechanics and Biomedical Engineering

Publication details, including instructions for authors and subscription information:
http://www.tandfonline.com/loi/gcmb20

Hip joint centre localisation with an unscented Kalman filter

Elena De Momi[a], Elisa Beretta[a] & Giancarlo Ferrigno[a]

[a] NearLab, Bioengineering Department, Politecnico di Milano, Milan, Italy

Published online: 30 Mar 2012.

To cite this article: Elena De Momi, Elisa Beretta & Giancarlo Ferrigno (2013) Hip joint centre localisation with an unscented Kalman filter, Computer Methods in Biomechanics and Biomedical Engineering, 16:12, 1319-1329, DOI: 10.1080/10255842.2012.670852

To link to this article: http://dx.doi.org/10.1080/10255842.2012.670852

Computer Methods in Biomechanics and Biomedical Engineering, 2013
Vol. 16, No. 12, 1319–1329, http://dx.doi.org/10.1080/10255842.2012.670852

Hip joint centre localisation with an unscented Kalman filter

Elena De Momi*, Elisa Beretta and Giancarlo Ferrigno

NearLab, Bioengineering Department, Politecnico di Milano, Milan, Italy

(*Received 21 October 2011; final version received 26 February 2012*)

The accurate estimation of the hip joint centre (HJC) in gait analysis and in computer assisted orthopaedic procedures is a basic requirement. Functional methods, based on rigid body localisation, assessing the kinematics of the femur during circumduction movements (pivoting) have been used for estimating the HJC. Localising the femoral segment only, as it is usually done in total knee replacement procedure, can give rise to estimation errors, since the pelvis, during the passive pivoting manoeuvre, might undergo spatial displacements. This paper presents the design and test of an unscented Kalman filter that allows the estimation of the HJC by observing the pose of the femur and the 3D coordinates of a single marker attached to the pelvis. This new approach was validated using a hip joint mechanical simulator, mimicking both hard and soft tissues. The algorithm performances were compared with the literature standards and proved to have better performances in case of pelvis translation greater than 8 mm, thus satisfying the clinical requirements of the application.

Keywords: hip joint centre; computer assisted orthopaedic surgery; total knee replacement

Introduction

Ideally, the hip joint can be modelled as a ball and socket joint. The exact localisation of the hip joint centre (HJC), i.e. under the above assumption, the centre of rotation (CoR) about which the femur rotates relative to the pelvis (Cappozzo 1984), has great importance in gait analysis and in navigated surgical interventions.

Indeed lower limb movement analysis protocol in gait analysis requires the determination of the location of the HJC (Cappozzo et al. 1995; Andriacchi et al. 1998; Della Croce et al. 1999; Cereatti et al. 2007; Corazza et al. 2007) to estimate the hip joint movements (Stagni et al. 2000). On the other hand, in computer assisted orthopaedic surgery procedures, the HJC determination allows the estimation of the femoral mechanical axis, during total knee arthroplasty (TKA; Gonzalez and Mekhail 2004; Kinzl et al. 2004; Haaker et al. 2005; De Momi et al. 2008), of the position of the acetabular component, during total hip arthroplasty (Jaramaz et al. 1998; Wolf et al. 2005; Wixson 2008), and of the femoral neck axis during hip resurfacing (Barrett et al. 2007).

HJC position estimation methods can be based on regression techniques using external landmarks (Kadaba et al. 1990; Seidel et al. 1995; Vaughan et al. 1999; Bush and Gutowski 2003; Weinhandl and O'Connor 2010), based on medical images, using 2D (Bell et al. 1990; Dennis et al. 1998) or 3D datasets (Kirkwood et al. 1999; Hube et al. 2003; Harrington et al. 2007; Lin et al. 2008; Peters et al. 2010) or rely on a kinematic approach (formal methods) where the femur is pivoted relative to the pelvic acetabulum (Stindel 2005) and which can be further split in *sphere fitting* methods and *coordinate transformation* methods (Ehrig et al. 2006).

Focussing on the formal methods, the HJC is computed by *sphere fitting*, as the centre of the sphere that fits the trajectory of marker positions in the least square sense (Cappozzo 1984; Piazza et al. 2001), quartic best sphere fitting procedure (Gamage and Lasenby 2002) and planes perpendicular to marker trajectories (Halvorsen et al. 1999). With any reasonable initial estimate for the position of the rotation centre, these techniques were comparably accurate and effective. In the *coordinate transformation* approach, the fixed distance between markers attached on the same rigid body (joint) allows the definition of local coordinate systems (Marin et al. 2003; Piazza et al. 2004; Ehrig et al. 2006; Siston and Delp 2006; Heller et al. 2011). Considering spatial relations among each rigid body for all the time frames of the movement acquisition, the HJC can be therefore computed with a least square approach. Such methods are reported to be less influenced by displacements of the pelvis during the pivoting movement (Lopomo et al. 2010) with respect to the sphere fitting methods.

*Corresponding author. Email: elena.demomi@polimi.it

The validation of all the aforementioned geometrical methods encompasses:

(1) Models and numerical simulations using virtual joints (Gamage and Lasenby 2002; Halvorsen et al. 2005; Camomilla et al. 2006; Ehrig et al. 2006) by adding noise which accounts for the measurement noise and possible soft tissue artefacts. Using virtual models, the exact location of the HJC is known, but simulations are only an approximation of the motion resulting from the passive pivoting manoeuvre.
(2) Physical models as mechanical linkage (Piazza et al. 2001, 2004; Siston and Delp 2006; Cereatti et al. 2009), where acquired data are corrupted by photogrammetric noise. Such models represented the hip joint as a perfect sphere and did not allow any movement of what was considered the global reference frame (RF), which was coincident with the pelvis model.
(3) Human studies (*ex vivo* or *in vivo*). In tests performed on living humans, the true HJC localisation can be measured (Leardini et al. 1999), if, for example, US images of the subject are acquired (Hicks and Richards 2005), or unknown (Piazza et al. 2004; Schwartz and Rozumalski 2005; Lempereur et al. 2011). Studies on cadavers (Picard et al. 2007; Cereatti et al. 2009; De Momi et al. 2009; Lopomo et al. 2010) allow evaluating the estimated HJC localisation with respect to the anatomical or functional 'true' position.

The unwanted motion of the pelvis during the pivoting manoeuvre represents a systematic source of error, which affects in particular the sphere fitting approach (Lopomo et al. 2010). Methods based on coordinates transformations are less affected by the pelvis bone displacement, since the least square approach allows the best fitting of the rigid body pose trajectory. It has to be noted that in the study of Lopomo et al. (2010) the pelvis was rigidly fixed to the table using pins. Also, Mihalko et al. (2006) showed that, in general, the absence of the pelvic tracker did not influence the total knee replacement (TKR) prosthesis alignment; nevertheless the errors in the HJC estimation are not negligible. In case the pelvis is passively moved during the pivoting manoeuvre, the HJC location estimation is highly affected.

Kalman filters have already been used for estimating the motion of hidden body segments using skin markers (Cerveri et al. 2003; Halvorsen et al. 2005; Senesh and Wolf 2009). Kalman filter proved to be robust in reconstructing the rigid body poses in case of temporary missing data (Halvorsen et al. 2008).

In order to tackle the problem of HJC position estimation in case of pelvis displacement, in this paper we present an innovative approach using an unscented Kalman filter (UKF). Julier and Uhlman demonstrated the performance of the UKF in the context of state estimation for nonlinear control (Julier et al. 1995, 2000; Julier and Uhlmann 1997). The algorithm was experimentally validated, using a hip phantom resembling the orthopaedic intra-operative settings, and the performances were compared with the algorithms proposed by Siston and Delp (2006), which is currently the most robust and reliable algorithm easily applicable to orthopaedic navigation systems (Lopomo et al. 2010), and with the algorithm proposed by De Momi et al. (2009) based on a Monte Carlo simulation.

Methods

The kinematic model and model calibration

The kinematic chain represented by the pelvis and the femur is a set of two segments linked by a joint. As presented in the findings of Halvorsen et al. (2008), the hip joint model can be represented as a spherical joint. The coordinate transformation from the proximal (pelvis) to the distal (femur) is a 4×4 matrix. For describing the kinematic chain, four RFs were defined (Figure 1):

(1) Laboratory (L) RF ($\mathbf{RF_L}$): RF with the origin in (0, 0, 0).
(2) Pelvis (P) RF ($\mathbf{RF_P}$): RF with the origin coincident with the pelvis anterior superior iliac spine (ASIS) and the Z axis directed toward the HJC.
(3) HJC sphere fitting RF ($\mathbf{RF_{HJC}}$): RF with the origin coincident with the centre of the femoral head.

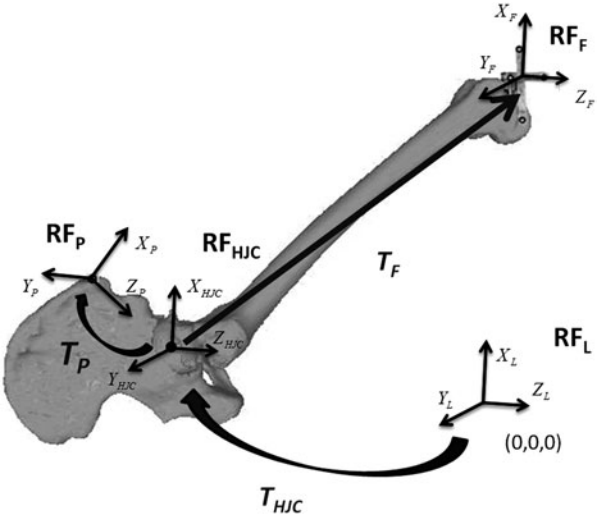

Figure 1. The hip and femur kinematic model, RFs and spatial transformations are indicated.

(4) Femoral (F) RF ($\mathbf{RF_F}$): RF with the origin coincident with a distal point of the femur.

The transformations relating the aforementioned RFs are the following:

(1) $\mathbf{RF_L}$ to $\mathbf{RF_{HJC}}$ ($\boldsymbol{T_{HJC}}$). Rotations of $\boldsymbol{T_{HJC}}$ in space were expressed using the unit quaternion-based rotation representation:

$$\begin{bmatrix} x_{\mathrm{HJC}} & y_{\mathrm{HJC}} & z_{\mathrm{HJC}} & q^0_{\mathrm{HJC}} & q^x_{\mathrm{HJC}} & q^y_{\mathrm{HJC}} & q^z_{\mathrm{HJC}} \end{bmatrix}.$$

(2) $\mathbf{RF_{HJC}}$ to $\mathbf{RF_P}$ ($\boldsymbol{T_P}$). $\boldsymbol{T_P}$ transformation matrix has 3 degrees of freedom (DoFs): two rotation (ϑ and η) around, respectively, Z and Y' axes, expressed as Euler angles, and a translation (D) along the Z' direction.

(3) $\mathbf{RF_{HJC}}$ to $\mathbf{RF_F}$ ($\boldsymbol{T_F}$). This transformation matrix has 3 DoFs i.e. the translation vector from the $\mathbf{RF_{HJC}}$ origin to the $\mathbf{RF_F}$ origin $\lfloor L_x \quad L_y \quad L_z \rfloor$.

The configuration vector (φ), describing the model kinematics, is therefore expressed by 13 elements (12 DoFs):

$$\varphi = \begin{pmatrix} x_{\mathrm{HJC}} & y_{\mathrm{HJC}} & z_{\mathrm{HJC}} & q^0_{\mathrm{HJC}} & q^x_{\mathrm{HJC}} & q^y_{\mathrm{HJC}} & q^z_{\mathrm{HJC}} \\ L_x & L_y & L_z & D & \vartheta & \eta \end{pmatrix} \quad (1)$$

where x_{HJC}, y_{HJC}, z_{HJC}, q^0_{HJC}, q^x_{HJC}, q^y_{HJC} and q^z_{HJC} are the 7 parameters (6 DoFs) defining $\boldsymbol{T_{HJC}}$, L_x, L_y, L_z define $\boldsymbol{T_P}$ and (D, θ, η) define $\boldsymbol{T_F}$.

State space model

We used the discrete time state space model:

$$\mathbf{x}(k+1) = F\mathbf{x}(k) + v(k), \quad (2)$$

$$\mathbf{y}(k) = h(\mathbf{x}(k)) + e(k), \quad (3)$$

where $\mathbf{x}(k)$ is the state vector, $\mathbf{y}(k)$ is the model output, $\nu(k)$ and $e(k)$ are the process and the measurement noise, respectively.

The state consists of the configuration vector (φ) (Equation (4)), of which some variables (from 1st to 7th and variables 12th and 13th) have dynamics (we adopted a second order model (Cerveri et al. 2003) so the first and second derivatives of the variables will appear as further state variables). The variables without any dynamics are (L_x, L_y, L_z, D).

$$\mathbf{x} = \begin{bmatrix} x_{\mathrm{HJC}} \\ \dot{x}_{\mathrm{HJC}} \\ \ddot{x}_{\mathrm{HJC}} \\ y_{\mathrm{HJC}} \\ \dot{y}_{\mathrm{HJC}} \\ \ddot{y}_{\mathrm{HJC}} \\ z_{\mathrm{HJC}} \\ \dot{z}_{\mathrm{HJC}} \\ \ddot{z}_{\mathrm{HJC}} \\ q^0_{\mathrm{HJC}} \\ \dot{q}^0_{\mathrm{HJC}} \\ \ddot{q}^0_{\mathrm{HJC}} \\ q^x_{\mathrm{HJC}} \\ \dot{q}^x_{\mathrm{HJC}} \\ \ddot{q}^x_{\mathrm{HJC}} \\ q^y_{\mathrm{HJC}} \\ \dot{q}^y_{\mathrm{HJC}} \\ \ddot{q}^y_{\mathrm{HJC}} \\ q^z_{\mathrm{HJC}} \\ \dot{q}^z_{\mathrm{HJC}} \\ \ddot{q}^z_{\mathrm{HJC}} \\ L_x \\ L_y \\ L_z \\ D \\ \vartheta \\ \dot{\vartheta} \\ \ddot{\vartheta} \\ \eta \\ \dot{\eta} \\ \ddot{\eta} \end{bmatrix}. \quad (4)$$

The state transition function $F(\cdot)$ (prediction of the next state given the current state) equation is a second order Taylor series (Cerveri et al. 2003).

The process noise is supposed to have a zero-mean Gaussian distribution $\boldsymbol{N}(0, \boldsymbol{Q})$, where $\boldsymbol{Q}$ is the covariance matrix of the process noise (Fioretti and Jetto 1989). The value σ_q^2, which defines the covariance of the noise process for each state variable q, was empirically set (Table 1).

Table 1. State error covariance and measurement error covariance values.

State noise covariance **Q**		Measurement noise covariance **R**	
$\sigma_{q,\mathrm{HJC}}$	$10^4\,\mathrm{mm}^2$ (x, y, z) 10^4 (*quaternion elements*)	$\sigma_{r,\mathrm{DRF}}$	$10^{-2}\,\mathrm{mm}^2$ (x, y, z) 10^{-3} (*quaternion elements*)
$\sigma_{q,L}$	$10^{-7}\,\mathrm{mm}^2$	$\sigma_{r,\mathrm{M}}$	$0.15\,\mathrm{mm}^2$
$\sigma_{q,D}$	$10^{-7}\,\mathrm{mm}^2$		
$\sigma_{q,\vartheta,\eta}$	$10^4\,\mathrm{rad}^2$		

Observations are the transformation matrix of a dynamic reference frame (DRF) rigidly connected to the femur and the 3D coordinates of a marker (M) attached to the pelvis (ASIS). The $h(\cdot)$ function is therefore non-linear.

The observation vector **y** is:

$$\mathbf{y} = \begin{bmatrix} x_{\mathrm{DRF}} \\ y_{\mathrm{DRF}} \\ z_{\mathrm{DRF}} \\ q^0_{\mathrm{DRF}} \\ q^x_{\mathrm{DRF}} \\ q^y_{\mathrm{DRF}} \\ q^z_{\mathrm{DRF}} \\ x_{\mathrm{M}} \\ y_{\mathrm{M}} \\ z_{\mathrm{M}} \end{bmatrix}, \tag{5}$$

where $\begin{bmatrix} x_{\mathrm{DRF}} & y_{\mathrm{DRF}} & z_{\mathrm{DRF}} & q^0_{\mathrm{DRF}} & q^x_{\mathrm{DRF}} & q^y_{\mathrm{DRF}} & q^z_{\mathrm{DRF}} \end{bmatrix}$ describes the pose of the femur and $\begin{bmatrix} x_{\mathrm{M}} & y_{\mathrm{M}} & z_{\mathrm{M}} \end{bmatrix}$ are the 3D coordinates of the marker attached to the ASIS in $\mathbf{RF_L}$.

The covariance matrix **R** of the additive measurement noise $e(t)$, describes a time-varying isotropic measurement noise. The value σ_r^2, which defines the covariance of the measurement noise for each observation, was empirically set (Table 1).

Unscented Kalman filtering

The UKF algorithm encompasses a linear state prediction and the following state update based on the unscented transform using the Free Software Foundation, Inc. (Boston, MA, USA; Julier and Uhlmann 1997). The measurement noise was propagated through the non-linear measurement function $h(\cdot)$. The estimate of the actual state ($\hat{\mathbf{x}}_k$) and the covariance matrix ($\mathbf{P}_k$) are defined as:

$$\hat{\mathbf{x}}_k = E[\mathbf{x}_k], \tag{6}$$

$$\mathbf{P}_k = E[(\mathbf{x}_k - \hat{\mathbf{x}}_k)(\mathbf{x}_k - \hat{\mathbf{x}}_k)^T] \tag{7}$$

with k the iteration number (time step $k\Delta t$). The predicted state $\mathbf{x}_k^-$ and its covariance $\mathbf{P}_k^-$ are defined as:

$$\mathbf{x}_k^- = F\hat{\mathbf{x}}_{k-1}, \tag{8}$$

$$\mathbf{P}_k^- = F\mathbf{P}_{k-1}F^T + \mathbf{Q}. \tag{9}$$

The sigma points ($\mathbf{X}_k^-$) of the predicted state variables are:

$$\mathbf{X}_k^{-(0)} = \mathbf{x}_k^-, \tag{10}$$

$$\mathbf{X}_k^{-(i)} = \mathbf{x}_k^- + \left[\sqrt{(n+\lambda)\mathbf{P}_k^-}\right]_i, \quad i = 1, \ldots, n, \tag{11}$$

$$\mathbf{X}_k^{-(i)} = \mathbf{x}_k^- - \left[\sqrt{(n+\lambda)\mathbf{P}_k^-}\right]_i, \quad i = n+1, \ldots, 2n, \tag{12}$$

where n is the state vector dimension ($n = 31$), $[\sqrt{(n+\lambda)\mathbf{P}_k^-}]_i$ is the ith column of the square root covariance matrix, computed as the lower triangular Cholesky factorisation, and λ is a scale parameter (van de Merwe and Wan 2001), defined as:

$$\lambda = \alpha^2(n+g) - n. \tag{13}$$

The constant α refers to the spread of sigma points around $\mathbf{x}_k^-$ (usually $0 < \alpha < 1$, in this work $\alpha = 0.5$) and g is set equal to $n - 3$ (Julier et al. 1995).

Two different weights $W_m^{(i)}$ and $W_c^{(i)}$ are defined for each sample i of the dataset $\mathbf{X}_k^-$:

$$W_m^0 = \frac{\lambda}{(n+\lambda)}, \tag{14}$$

$$W_c^0 = \frac{\lambda}{(n+\lambda)} + (1 - \alpha^2 - \beta), \tag{15}$$

$$W_m^{(i)} = W_c^{(i)} = \frac{1}{\{2(n+\lambda)\}}, \quad i = 1, \ldots, 2n, \tag{16}$$

where for a Gaussian distribution, $\beta = 2$ (Julier et al. 1995).

The sigma points $\mathbf{X}_k^{(i)}$ are propagated through the non-linear observation model $h(\cdot)$ to estimate the mean ($\boldsymbol{\mu}_k$), the covariance matrix ($\mathbf{S}_k$) of the predicted observations $\mathbf{Y}_k^{(i)}$ and the cross-covariance matrix ($\mathbf{C}_k$) between the predicted

observations and the state:

$$\mathbf{Y}_k^{(i)} = h\left(\mathbf{X}_k^{-(i)}\right), \quad i = 0, \ldots, 2n, \tag{17}$$

$$\boldsymbol{\mu}_k = \sum_{i=0}^{2n} W_m^{(i)} \mathbf{Y}_k^{(i)}, \tag{18}$$

$$\mathbf{S}_k = \sum_{i=0}^{2n} W_c^{(i)} \left(\mathbf{Y}_k^{(i)} - \boldsymbol{\mu}_k\right)\left(\mathbf{Y}_k^{(i)} - \boldsymbol{\mu}_k\right)^T + R_k, \tag{19}$$

$$\mathbf{C}_k = \sum_{i=0}^{2n} W_c^{(i)} \left(\mathbf{X}_k^{(i)} - \mathbf{x}_k^-\right)\left(\mathbf{Y}_k^{(i)} - \boldsymbol{\mu}_k\right)^T. \tag{20}$$

The state estimation ($\hat{\mathbf{x}}_k$) and the covariance matrix estimation ($\mathbf{P}_k$) are then updated through the computation of the Filter Gain ($\mathbf{K}_k$):

$$\mathbf{K}_k = \mathbf{C}_k \mathbf{S}_k^{-1}, \tag{21}$$

$$\hat{\mathbf{x}}_k = \mathbf{x}_k^- + \mathbf{K}_k(\mathbf{y}_k - \boldsymbol{\mu}_k), \tag{22}$$

$$\mathbf{P}_k = \mathbf{P}_k^- + \mathbf{K}_k \mathbf{S}_k \mathbf{K}_k^T. \tag{23}$$

Initialisation

The algorithm was initialised using the method proposed by Siston and Delp (2006), which estimates:

(1) the position of the HJC in the $\mathbf{RF_F}$: (L_{x0} L_{y0} L_{z0}),
(2) the initial position of the HJC in the $\mathbf{RF_L}$: $\mathbf{HJC}_0 = (\, x_{\mathrm{HJC0}} \quad y_{\mathrm{HJC0}} \quad z_{\mathrm{HJC0}} \,)$.

The 13 unknown elements of the configuration vector φ_0 were estimated using the DRF orientation (q^0_{DRF1} q^x_{DRF1} q^y_{DRF1} q^z_{DRF1}) at the first time frame and the ASIS marker initial position $\mathbf{M}_1(\, x_{\mathrm{M1}} \quad y_{\mathrm{M1}} \quad z_{\mathrm{M1}} \,)$:

$$\begin{aligned} q^0_{\mathrm{HJC0}} &= q^0_{\mathrm{DRF1}}, \\ q^x_{\mathrm{HJC0}} &= q^x_{\mathrm{DRF1}}, \\ q^y_{\mathrm{HJC0}} &= q^y_{\mathrm{DRF1}}, \\ q^z_{\mathrm{HJC0}} &= q^z_{\mathrm{DRF1}}, \end{aligned} \tag{24}$$

$$D_0 = \|\mathbf{HJC}_0 - \mathbf{M}_1\|, \tag{25}$$

$$\vartheta_0 = \begin{cases} \arctan\left(\frac{m_y}{m_x}\right), & m_x < 0, \\ \arctan\left(\frac{m_y}{m_x}\right) + \pi, & m_x \geq 0, \end{cases} \tag{26}$$

with:

$$m_i = \frac{|i_{\mathrm{HJC0}} - i_{\mathrm{M1}}|}{D_0}, \quad i = x, y, z, \tag{27}$$

$$\eta_0 = \arccos(m_z). \tag{28}$$

The initial derivatives of each variable are set to zero.

Table 2. Initial state covariance matrix tuning values.

Initial state covariance $\mathbf{P}_0$	
$\sigma_{p,\mathrm{HJC}}$	$10^6\,\mathrm{mm}^2$ (x, y, z) 10^6 (*quaternion elements*)
$\sigma_{p,L}$	$10^2\,\mathrm{mm}^2$
$\sigma_{p,D}$	$10^2\,\mathrm{mm}^2$
$\sigma_{p,\vartheta,\eta}$	$10^6\,\mathrm{rad}^2$

The initial state covariance matrix ($\mathbf{P}_0$) is a diagonal matrix with initial tuning values reported in Table 2.

The experimental protocol

In order to validate the proposed method, a hip joint phantom was built using Sawbones® models of pelvis and femur. In order to mimic the spherical joint, a spherical coupling was realised using semi-rigid foam material. Elastic strips modelled the joint tendons and ligament actions. The upper body part was modelled with a pre-loaded mass-spring system (Figure 2). The hip phantom acetabular radius was 23.17 mm (root mean square error (RMSE) 0.47 mm), whereas the femoral head radius was 21.70 mm (RMSE 0.39 mm).

The Certus optical system (NDI, Waterloo, Ontario, Canada) was used to acquire the 3D pose of a custom built DRF rigidly attached to the femur (femur DRF). The DRF carried four Infra Red Emitting Diodes (IREDs) in a planar configuration (pelvis DRF). Four IREDs were attached to the pelvis bone, respectively, on the right ASIS, on the pubic tubercle, on the left iliac fossa and on the 16th sacral vertebra (Figure 2). Note that these latter three IREDs are used only for test purposes and they are not meant to be used in the clinical implementation of the method where only the ASIS point is required. The femoral head ($\mathrm{HJC_F}$) and the acetabular ($\mathrm{HJC_A}$) anatomical centres ('true centres') were determined fitting a sphere on the point cloud acquired on the femoral head and on the acetabulum, using a standard least square approach (Golub and Van Loan 1996), identifying also the corresponding spherical radii.

Circumduction movements (46 repetitions) were performed by an operator, who pivoted the femoral bone around the hip. The circumduction range of motion (RoM) was computed in the anterior–posterior (AP) and medial–lateral (ML) anatomical planes (Wu et al. 2002). An anatomic (A) RF ($\mathbf{RF_A}$) was defined, with the origin coincident with the $\mathrm{HJC_A}$, Z axis passing through the two ASIS (pointing from left to right) and X axis passing through the mean point of the posterior superior iliac spines (PSIS) and the ASIS mean point (as shown in Figure 3).

The RoM in the AP plane (α_{AP}) is:

$$\alpha_{\mathrm{AP}} = \arctan\left(-\frac{x_{\mathrm{DRF_A}}}{y_{\mathrm{DRF_A}}}\right)$$

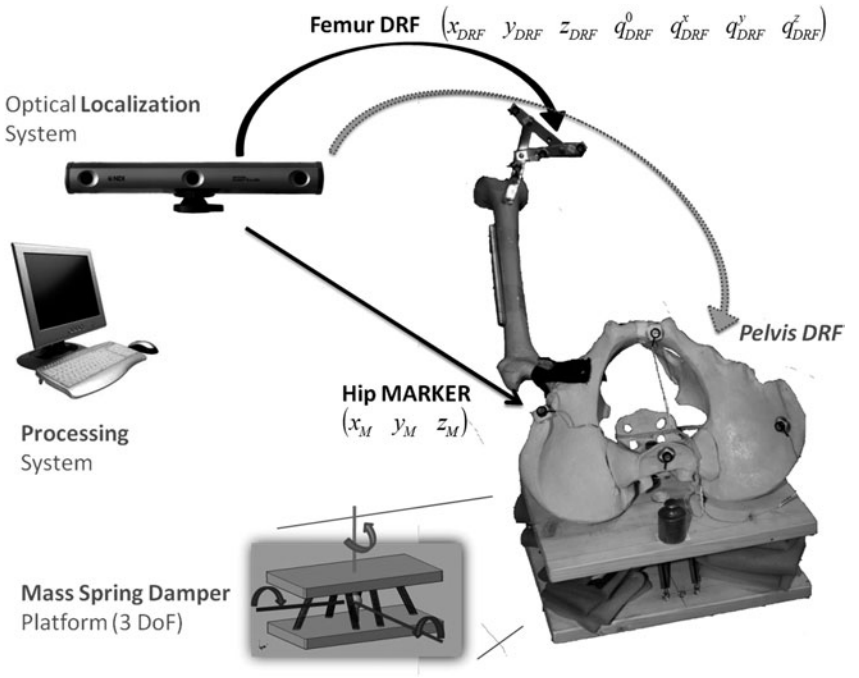

Figure 2. Hip joint phantom and the experimental set-up.

and the RoM in the ML plane (β_{AP}) is:

$$\beta_{AP} = \arctan\left(\frac{z_{DRF_A}}{y_{DRF_A}}\right).$$

During the passive movements the circumduction RoM were in the range 10°–80° ($10° < \Delta\alpha_{AP} < 60°$, $10° < \Delta\beta_{AP} < 80°$), the movement velocity in the range 80–1200 mm/s and the HJC translation (Tr_{HJC}) in the range 0.7–15 mm. Data were acquired at 200 Hz frame rate, each acquisition lasting 60 s (Figure 3).

We compared the UKF approach with standard methods in the literature. Among these, the pivoting (P) method, proposed by (Siston and Delp 2006), is considered to be the most robust and reliable for orthopaedic navigation procedures (Ehrig et al. 2006). Better performances in terms of accuracy were obtained in the findings of De Momi et al. (2009) with trials on cadaver specimens using a Monte-Carlo pivoting (MCP) approach. The accuracy of the estimation was assessed computing the Euclidean distance between the HJC_F and the HJC estimated using functional algorithms. Percentiles of the distances distribution were also computed.

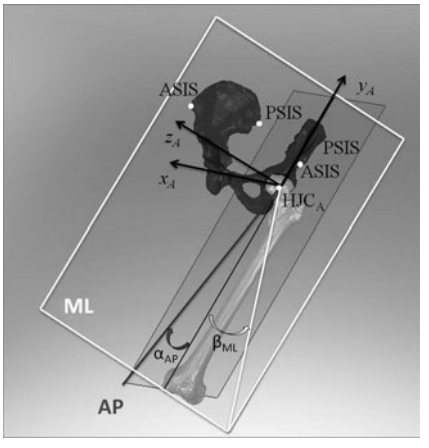

Figure 3. AP and ML planes RoM estimation (α_{AP} and β_{ML}), ASIS and PSIS landmarks are shown, together with the HJC_A in $\mathbf{RF_A}$.

Performances of the P, MCP and UKF algorithm were compared using

(1) The Wilcoxon paired test ($p < 0.05$). In order to evaluate the performances of each algorithm with respect to the motion characteristics, the MannWhitney test was used ($p < 0.05$).
(2) The correlation coefficient (Pearson correlation coefficient, $p < 0.05$) among the accuracy of the three algorithms and:
- the circumduction RoM;
- the circumduction movement velocity (Vel);
- the HJC induced translation (Tr_{HJC}).

Results

Figure 4 shows the results of the three methodologies (P, MCP and UKF) in terms of HJC estimation accuracy. Results are expressed as a function of the acetabulum translation (Tr_{HJC}) and grouped accordingly as 'small

RoM' ($\Delta\alpha_{AP} < 36^\circ$ $\Delta\beta_{ML} < 50^\circ$) (Figure 4(a)) or 'wide RoM' ($\Delta\alpha_{AP} > 36^\circ$ $\Delta\beta_{ML} > 50^\circ$; Figure 4(b)), resulting in two equally numerous populations. In both cases, a better behavior of the HJC estimate by using UKF is found when Tr_{HJC} is greater than 8 mm. Even if the different performances between MCP and UKF are not statistically significant ($p = 0.07$) in case the pelvis movement is greater than 8 mm, the median error of UKF is less than 50% of the MCP error (about 10 mm). All the methods are strictly dependent on the HJC translation (Tr_{HJC}) during the pivoting manoeuvre, even if UKF is less influenced (Table 3). Pivoting and MCP are not influenced by the movement RoM, while localisation errors for UKF are smaller in case of large movements.

Figure 5 shows the HJC localisation accuracy of the UKF algorithm alone as a function of the pivoting movement velocity. As shown, the algorithm performances depend on the movement velocity in case of pelvis displacement greater than 2.5 mm, also only the MCP algorithm is negatively influenced by the movement velocity (Table 3).

Figure 6 shows data acquired during the pivoting and the estimated HJC trajectory. The UKF algorithm allows tracking the real position of the HJC better than the other algorithms.

Discussion

The requirement for accuracy in the HJC localisation depends on the application scenario that can be gait analysis or computer assisted orthopaedic procedures. As

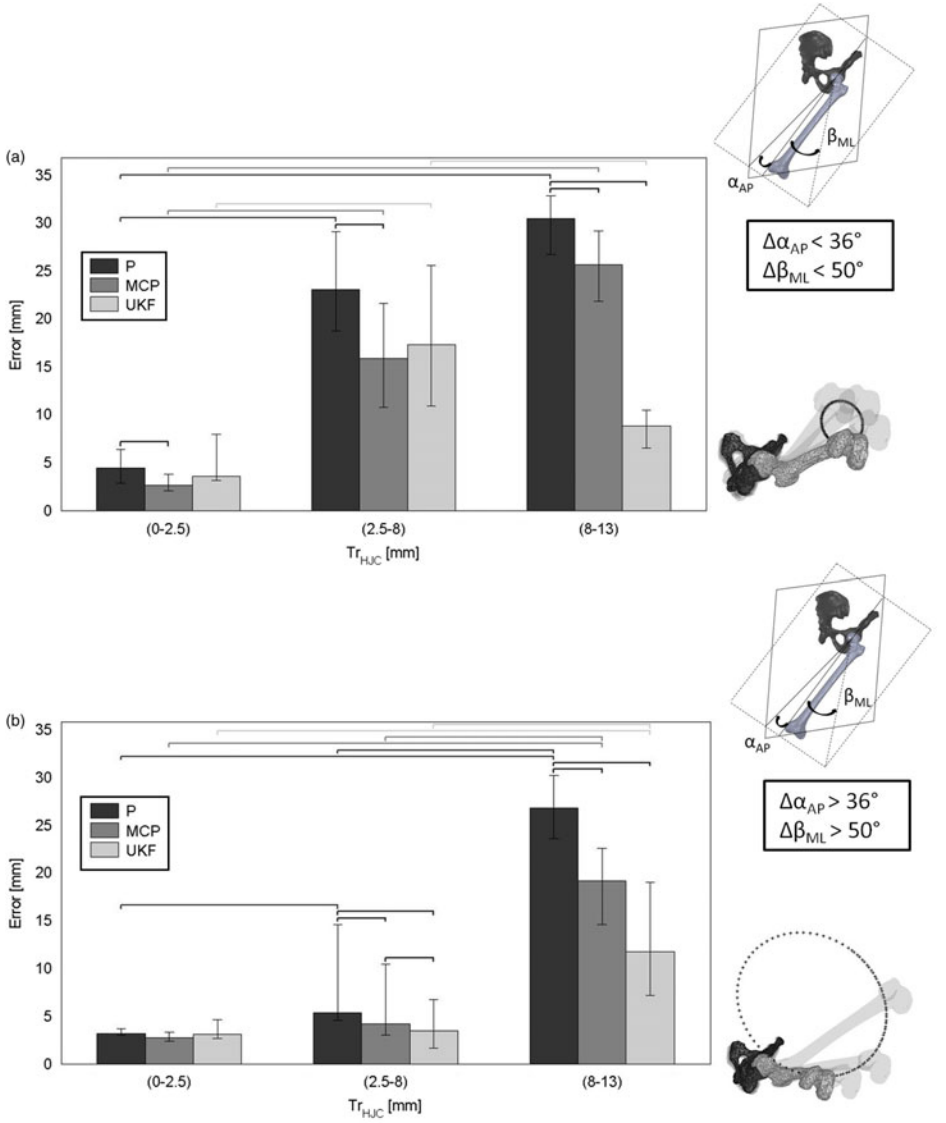

Figure 4. Evaluation of the HJC localisation accuracy using the three algorithms (P, MCP and UKF): (a) when the ROM is less than 36° and 50° respectively in AP and ML planes and (b) when the ROM is greater than 36° and 50° respectively in AP and ML planes. Intra-group (Wilcoxon paired test, $p < 0.05$) and inter-group (Mann–Withney, $p < 0.05$) comparisons were carried out.

Table 3. Pearson correlation coefficients (*, p value < 0.05).

	Pivoting	MCP	UKF
Tr_{HJC}	0.815*	0.804*	0.282*
RoM_{AP}	−0.187	−0.140	−0.432*
RoM_{ML}	−0.126	−0.054	−0.427*
Vel	0.010	−0.083	0.273*

an example, TKA clinical assessment tolerates ±3° of varus/valgus for the alignment of the mechanical axis in the frontal plane. Nearly 3 cm of inaccuracy in the HJC estimation lead to 1.7° alignment error (Lopomo et al. 2010). Smaller errors can be tolerated in hip resurfacing interventions, where the estimation of the femoral neck axis is necessary in order to correctly align the femoral prosthesis component.

During TKA procedures, an optical DRF is screwed in the distal bone and pose data are acquired during functional movements. Several methodologies for the HJC localisation have been reported in the literature, the most acknowledged method for navigation procedure is proposed by Siston and Delp (2006).

Nevertheless, all the methodologies presented do not extensively analyse the estimation perturbation introduced by the pelvis displacement during the passive pivoting manoeuvre. Even if some authors suggested that the pelvic tracker did not significantly improve the HJC localisation accuracy (Mihalko et al. 2006), it is well recognised that the measurement of the pelvis movement is necessary in order to raise warnings on the HJC automatic computation, which could result to be inaccurate if the pelvis has undergone a translation movement during the acquisition. An estimate of such displacement can be obtained computing the instantaneous positions of the HJC, as

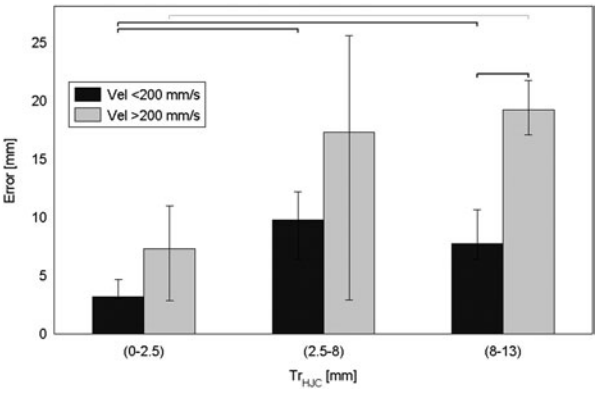

Figure 5. Evaluation of the HJC localisation accuracy using UKF algorithm with respect to the movement velocity. Intra-group (Wilcoxon paired test, $p < 0.05$) and inter-group (Mann–Withney test was used, $p < 0.05$) comparisons were carried out.

presented by De Momi et al. (2009). Having a rough estimate of the HJC it is possible to track the motion of the rotation centre in time, therefore the UKF based proposed methodology is particularly suitable in the cases where the pelvis had undergone a significant displacement. The innovative method presented in this paper allows the accurate localisation the HJC even if the pelvis translations are greater than 1 cm in magnitude, thus overcoming what is stated in the findings of Stindel (2005), i.e. the displacement of the CoR during the acquisition motion cannot be modelled. The Kalman gain allows to estimate the movement of hidden segments (pelvis and femur), given observations on the pose of the femur and the 3D coordinates of a single marker attached to the pelvis and given the regularity of the motion (finite acceleration).

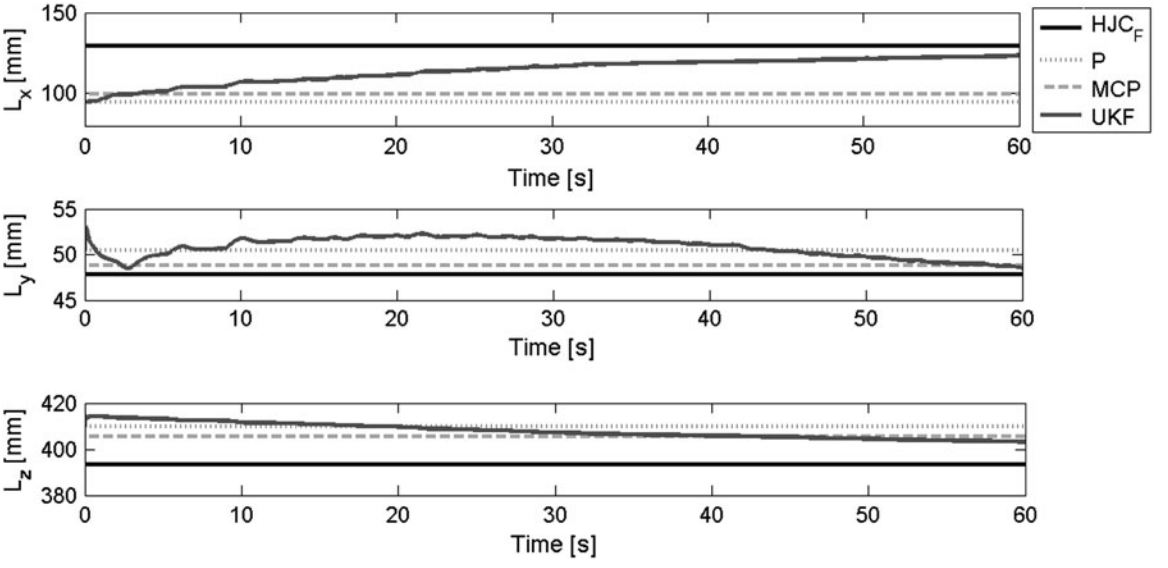

Figure 6. Trajectories of the estimated HJC in RF using the three algorithms (P, MCP and UKF). The 'true' trajectory (HJCF) is also shown.

The pelvis marker was thought to be attached to the ASIS where the skin artefact noise was low. With regard to the clinical application, when the pelvis is draped with sterile linens, we suggest to link a stick with two markers through elastic bands on the patient's pelvis and to estimate the 3D coordinates of the point. Since the algorithm requires only the position of the ASIS, it must be pointed out that the rotation of the stick around the fixation point does not create any error in its location. Furthermore two markers, aligned on the stick's longitudinal axis, are enough to localise the tip position. Such a point will be anyway subject to great noise artefacts, which are filtered out by the UKF approach.

Previous application of Kalman filter used to track the motion of hidden segments given the 3D positions of markers attached to the skin (Cerveri et al. 2003; Halvorsen et al. 2008) used the Extended Kalman filtering approach, where the $h(\cdot)$ function was numerically linearised. We chose to model our dynamic process using an UKF approach, since the state and observation noise distribution are supposed to be Gaussian and the $h(\cdot)$ function, which relates the state variables with the observations, is nonlinear.

Due to the necessity of tracking the pelvis motion, in order to know the exact position of the HJC during the pivoting maneuver, accurate testing can be performed using phantoms or cadavers. Tests *in vivo* can only report the methods' repeatability. Even if the assessment of the new methodology was limited to the hip phantom, the kinematical and mechanical characteristics resembled one of the normal hip joint (Cereatti et al. 2010; Lopomo et al. 2010). The hip has been modelled as a spherical joint in the studies of Cereatti et al. (2007), Halvorsen et al. (2008), Lopomo et al. (2010) even if Kang (2011) reported that considering the femoral head as a sphere can lead to calculation errors (Menschick 1997). The phantom analysis allowed us to repeat several experiments on the same testing material, which did not alter during time. Also, the pelvis displacement, which is the principal parameter against which we assessed the performances of our methodology, can be accurately measured and altered in a controlled way.

Results showed that the potentialities of the new approach with respect to literature are evident in particular if the pelvis translation is greater than 8 mm. The UKF algorithm performances depend on the femur velocity: better results are obtained if the pivoting speed is below 200 mm/s (tangential velocity). This can be due to the inability of the filter to track state variations at high frequencies and to the increase in the movement acquisition noise. Measurement noise tuning was performed considering the static noise claimed by the manufacturing company of the optical tracking system.

The work presented, though centred on orthopaedics, has potential impact in the biomechanics field also, since it is possible to accurately predict the position of CoR using partial information coming from markers placed on a single body segment. Further development of the configuration vector is required in this case and skin artefact effects have to be evaluated.

Further analysis on the acquired signals involves the design of particle filtering (Kotecha 2003) in order to better model the nonlinear process under investigation.

Notes

1. Email: elisa.beretta@mail.polimi.it
2. Email: giancarlo.ferrigno@polimi.it

References

Andriacchi TP, Alexander EJ, Toney MK, Dyrby C, Sum J. 1998. A point cluster method for *in vivo* motion analysis: applied to a study of knee kinematics. J Biomech Eng. 120:743–749.

Barrett A, Davies B, Gomes M, Harris S, Henckel J, Jakopec M, Kannan V, Rodriguez y Baena F, Cobb J. 2007. Computer-assisted hip resurfacing surgery using the Acrobot navigation system. Proc Inst Mech Eng H. 221(H7):773–785.

Bell AL, Pedersen DR, Brand RA. 1990. A comparison of the accuracy of several hip center location prediction methods. J Biomech. 23(6):617–621.

Bush TR, Gutowski PE. 2003. An approach for hip joint center calculation for use in seated postures. J Biomech. 36(11):1739–1743.

Camomilla V, Cereatti A, Vannozzi G, Cappozzo A. 2006. An optimized protocol for hip joint centre determination using the functional method. J Biomech. 39(6):1096–1106.

Cappozzo A. 1984. Gait analysis methodology. Hum Mov Sci. 3(1–2):27–50.

Cappozzo A, Catani F, Della Croce U, Leardini A. 1995. Position and orientation in space of bones during movement: anatomical frame definition and determination. Clin Biomech. 10(4):171–178.

Cereatti A, Camomilla V, Vannozzi G, Cappozzo A. 2007. Propagation of the hip joint centre location error to the estimate of femur vs pelvis orientation using a constrained or an unconstrained approach. J Biomech. 40(6):1228–1234.

Cereatti A, Donati M, Camomilla V, Margheritini F, Cappozzo A. 2009. Hip joint centre location: an *ex vivo* study. J Biomech. 42(7):818–823.

Cereatti A, Margheritini F, Donati M, Cappozzo A. 2010. Is the human acetabulofemoral joint spherical? J Bone Joint Surg Br. 92(2):311–314.

Cerveri P, Pedotti A, Ferrigno G. 2003. Robust recovery of human motion from video using Kalman filters and virtual humans. Hum Mov Sci. 22(3):377–404.

Corazza S, Mündermann L, Andriacchi T. 2007. A framework for the functional identification of joint centers using markerless motion capture, validation for the hip joint. J Biomech. 40(15):3510–3515.

Della Croce U, Cappozzo A, Kerrigan D. 1999. Pelvis and lower limb anatomical landmark calibration precision and its propagation to bone geometry and joint angles. Med Biol Eng Comput. 37(2):155–161.

De Momi E, Cerveri P, Ferrigno G. 2008. Navigation in computer assisted orthopaedic surgery. In: Dong F, Ghinea G, Chen SY, editors. User centered design for medical visualization. UK: Brunel University. p. 205–222.

De Momi E, Lopomo N, Cerveri P, Zaffagnini S, Safran M, Ferrigno G. 2009. *In-vitro* experimental assessment of a new robust algorithm for hip joint centre estimation. J Biomech. 42(8):989–995.

Dennis DA, Komistek RD, Stiehl JB, Walker SA, Dennis KN. 1998. Range of motion after total knee arthroplasty: the effect of implant design and weight-bearing conditions. J Arthroplasty. 13(7):748–752.

Ehrig RM, Taylor WR, Duda GN, Heller MO. 2006. A survey of formal methods for determining the centre of rotation of ball joints. J Biomech. 39(15):2798–2809.

Fioretti S, Jetto L. 1989. Accurate derivative estimation from noisy data: a state space approach. Int J Syst Sci. 20(1):33–53.

Gamage SSHU, Lasenby J. 2002. New least squares solutions for estimating the average centre of rotation and the axis of rotation. J Biomech. 35(1):87–93.

Golub GH, Van Loan CF. 1996. Matrix computations. New York: Johns Hopkins University Press.

Gonzalez MH, Mekhail AO. 2004. The failed total knee arthroplasty: evaluation and etiology. J Am Acad Orthop Surg. 12(6):436–446.

Haaker RG, Stockheim M, Kamp M, Proff G, Breitenfelder J, Ottersbach A. 2005. Computer-assisted navigation increases precision of component placement in total knee arthroplasty. Clin Orthop Relat Res 433:152–159.

Halvorsen K, Johnston C, Back W, Stokes V, Lanshammar H. 2008. Tracking the motion of hidden segments using kinematic constraints and Kalman filtering. J Biomech Eng. 130(1):011012.

Halvorsen K, Lesser M, Lundber A. 1999. A new method for estimating the axis of rotation and the center of rotation. J Biomech. 32(11):1221–1227.

Halvorsen K, Soderstrom T, Stokes V, Lanshammar H. 2005. Using an extended Kalman filter for rigid body pose estimation. J Biomech Eng. 127(3):475–483.

Harrington ME, Zavatsky AB, Lawson SEM, Yuan Z, Theologis TN. 2007. Prediction of the hip joint centre in adults, children, and patients with cerebral palsy based on magnetic resonance imaging, J Biomech. 40:595–602.

Heller MO, Kratzenstein S, Ehrig RM, Wassilew G, Duda GN, Taylor WR. 2011. The weighted optimal common shape technique improves identification of the hip joint center of rotation *in vivo*. J Orthop Res. 29(10):1470–1475.

Hicks JL, Richards JG. 2005. Clinical applicability of using spherical fitting to find hip joint centers. Gait Posture. 22(2):138–145.

Hube R, Birke A, Hein W, Klima S. 2003. CT-based and fluoroscopy-based navigation for cup implantation in total hip arthroplasty (THA). Surg Technol Int. 11:275–280.

Jaramaz B, DiGioia A, Blackwell M, Nikou C. 1998. Computer assisted measurement of cup placement in total hip replacement. Clin Orthop Relat Res 354:70–81.

Julier SJ, Uhlmann J. 1997. New extension of the Kalman filter to nonlinear systems. Proc. SPIE. July. 3086:182–193.

Julier SJ, Uhlmann J, Durrant-Whyte HF. 1995. A new approach for filtering nonlinear systems. In: Proceedings of the American Control Conference, Seattle WA, USA, p. 1628–32.

Julier SJ, Uhlmann J, Durrant-Whyte HF. 2000. A new method for the nonlinear transformation of means and covariances in filters and estimators. IEEE Trans Autom Control. 45(3):477–482.

Kadaba MP, Ramakrishnan HK, Wootten ME. 1990. Measurement of lower extremity kinematics during level walking. J Orthopaedic Res. 8(3):383–392.

Kang MJ. 2011. Determining the location of hip joint centre: application of a conchoid's shape to the acetabular cartilage surface of magnetic resonance images. Comput Methods Biomech Biomed Engin. 14(1):65–71.

Kinzl L, Gebhard F, Keppler P. 2004. Total knee arthroplasty – navigation as the standard. Chirurg. 75(10):976–981.

Kirkwood RN, Culham EG, Costigan P. 1999. Radiographic and non-invasive determination of the hip joint center location: effect on hip joint moments. Clin Biomech. 14(4):227–235.

Kotecha JH. 2003. Gaussian particle filtering. IEEE Trans Signal Processing. 51(10):2592–2601.

Leardini A, Cappozzo A, Catani F, Toksvig Larsen S, Petitto A, Sforza V, Cassanelli G, Giannini S. 1999. Validation of a functional method for the estimation of hip joint centre location. J Biomech. 32(1):99–103.

Lempereur M, Brochard S, Rémy-Néris O. Forthcoming 2011. Repeatability assessment of functional methods to estimate the glenohumeral joint centre. Comput Methods Biomech Biomed Engin.

Lin F, Lim D, Wixson RL, Milos S, Hendrix RW, Makhsous M. 2008. Validation of a computer navigation system and a CT method for determination of the orientation of implanted acetabular cup in total hip arthroplasty: a cadaver study. Clin Biomech. 23(8):1004–1011.

Lopomo N, Sun L, Zaffagnini S, Giordano G, Safran MR. 2010. Evaluation of formal methods in hip joint center assessment: an *in vitro* analysis. Clin Biomech. 25(3):206–212.

Marin F, Mannel H, Claes L, Dürselen L. 2003. Accurate determination of a joint rotation center based on the minimal amplitude point method. Comput Aided Surg. 8(1):30–34.

Mihalko WM, Phillips MJ, Fishkin Z, Krackow KA. 2006. Pelvic tracker effects on hip center accuracy using imageless navigation. Comput Aided Surg. 11(4):214–218.

Menschick F. 1997. The hip joint as a conchoid shape. J Biomech. 30(9):971–973.

Peters A, Baker R, Sangeux M. 2010. Validation of 3-D freehand ultrasound for the determination of the hip joint centre. Gait Posture. 31(4):530–532.

Piazza SJ, Erdemir A, Okita N, Cavanagh PR. 2004. Assessment of the functional method of hip joint center location subject to reduced range of hip motion. J Biomech. 37(3):349–356.

Piazza SJ, Okita N, Cavanagh PR. 2001. Accuracy of the functional method of hip joint center location: effects of limited motion and varied implementation. J Biomech. 34(7):967–973.

Picard F, Leitner F, Gregori A, Martin P. 2007. A cadaveric study to assess the accuracy of computer-assisted surgery in locating the hip center during total knee arthroplasty. J Arthroplasty. 22(4):590–595.

Schwartz MH, Rozumalski A. 2005. A new method for estimating joint parameters from motion data. J Biomech. 38(1):107–116.

Seidel GK, Marchinda DM, Dijkers M, Soutas-Little RW. 1995. Hip joint center location from palpable bony landmarks – a cadaver study. J Biomech. 28(8):995–998.

Senesh M, Wolf A. 2009. Motion estimation using point cluster method and Kalman filter. J Biomech Eng. 131(5):051008, (7 pages).

Siston RA, Delp SL. 2006. Evaluation of a new algorithm to determine the hip joint center. J Biomech. 39(1):125–130.

Stagni R, Leardini A, Cappozzo A, Benedetti M, Cappello A. 2000. Effects of hip joint centre mislocation on gait analysis results. J Biomech. 33(11):1479–1487.

Stindel E. 2005. Detection of the center of the hip joint in computer-assisted surgery: an evaluation study of the Surgetics algorithm. Comput Aided Surg. 10(3):133–139.

Vaughan CL, Davis BL, O'Connor J. 1999. Dynamics of human gait. Human Kinetics Publishers, pp. 22–44.

van der Merwe R, Wan E. May 2001. The square-root unscented kalman filter for state and parameter-estimation. ICASSP2011, Prague, Czech Republic, pp. 3461–3464.

Weinhandl JT, O'Connor KM. 2010. Assessment of a greater trochanter-based method of locating the hip joint center. J Biomech. 43:2633–2636.

Wixson RL. 2008. Computer-assisted total hip navigation. Inst Course Lect. 57:707–720.

Wolf A, DiGioia AM, III, Mor AB, Jaramaz B. 2005. A kinematic model for estimating cup alignment error during total hip arthroplasty. J Biomech. 33(11):2257–2265.

Wu G, Siegler S, Allard P, Kirtley C, Leardini A, Rosenbaum D, Whittle M, D'Lima DD, Cristofolini L, Witte H et al., 2002. ISB recommendation on definitions of joint coordinate system of various joints for the reporting of human joint motion – part I: ankle, hip, and spine. J Biomech. 35:543–548.